Int. j. adv. multidisc. res. stud. 2026; 6(3):1699-1712

Received: 01-05-2026
Accepted: 10-06-2026

International Journal of Advanced Multidisciplinary Research and Studies

ISSN: 2583-049X

DFT and Harmonic Force Fields of Species Derived from Potent Opioid Analgesic Hydrochloride Fentanyl Drug

[1] Elida Romano, [2] Maximiliano A Iramain, [3] María E Manzur, [4] María V Castillo, [5] Silvia Antonia Brandán

[1, 2, 3, 4, 5] Cátedra de Química General, Instituto de Química Inorgánica, Facultad de Bioquímica. Química y Farmacia, Universidad Nacional de Tucumán, Ayacucho 471, (4000) San Miguel de Tucumán, Tucumán, Argentina

Corresponding Author: **Silvia Antonia Brandán**

Abstract

In this work, B3LYP/6-311++G** and harmonic force fields calculations were combined to predict structural and vibrational properties of species derived from potent opioid fentanyl drug in the gas phase (GP) and in aqueous solution (AS). Hence, the expected 153, 156 and 159 normal vibration modes of base, cation and hydrochloride fentanyl were completely assigned and its scaled force constants reported. The studies of atomic charges evidence positive MK charges on N2 atoms confirming the protonation of cation and hydrochloride on the piperazine rings. A low gap value reveals that the hydrochloride form is the most reactive in AS (4.4545 eV) while in GP the cation is the less reactive (5.4940 eV). The absence in the experimental spectrum of a very strong IR band predicted for the hydrochloride form at 1913 cm^{-1}, suggests the presence of cation in the solid phase, as supported by the predicted UV-Vis spectra.

Keywords: Fentanyl, Structural Properties, SQMFF, Vibrational Analysis, B3LYP Calculations

1. Introduction

The potent opioid analgesic fentanyl drug is used in medicine to treat patients with chronic cancer pains because this drug is 50 and 100 times stronger than heroin and morphine, respectively [1-19]. In particular, fentanyl can be an abuse drug due to its effects, as tropane alkaloids when this drug is adulterated with other alkaloids, such as heroin or morphine becoming an illicit drug [20]. Therefore, its detection by different spectroscopic, electronic and other techniques is very important from different points of view such as forensic science and human health [3-19]. Thus, there are a vast number of studies reported in the literature on vibrational analysis using infrared and Raman spectra including using NMR, SERS, GC–Mass Spectrometry and Gas Chromatography–Infrared Spectroscopy and electrochemical techniques [3-19]. However, the most widely used technique to identify fentanyl and its derivatives is vibrational spectroscopy and, in many cases these experimental studies are shared with theoretical calculations [3-5, 7-9, 11-13, 15-18]. The experimental structure of fentanyl base was reported by Ogawa *et al.* [2] whereas Asadi *et al.* [3] described the synthesis and theoretical DFT study of base by NMR and IR spectroscopies [3]. In that study, there is a serious and grave error, because the fentanyl base was optimized with C_1 symmetry; however, the vibration modes are assigned taking into account a C_s symmetry instead C_1. Thus, the point group C_s has a plane of symmetry in addition to the identity and, the vibration modes have been classified as A' and A" when the structure with C_1 symmetry only has the identity as an element of symmetry. Here, that severe mistake in the assignments of base is corrected here. So far, experimental structural studies of base, cation and hydrochloride forms of fentanyl and, complete structural and vibrational studies of fentanyl have not been published yet. The structures of three species are shown in Fig. 1 where the cation shows its positive charge on N of piperidine ring. The IUPAC name of fentanyl is *N*-phenyl-*N*-[1-(2-phenylethyl)piperidin-4-yl]propanamide and, obviously the identifications of all the vibration modes are important to perform complete assignments, in particular, those related to three rings. Therefore, R1 is the piperidine ring; R2 is the phenyl-ethyl ring and R3, the *N*-phenyl ring. The aims of this work are, to optimize the structures of base, cation and hydrochloride fentanyl by using hybrid B3LYP/6-311++G(d,p) calculations [21, 22] and, after that, to perform the complete vibrational analyses of three species by using the scaled quantum mechanical force field (SQMFF) methodology [23-25]. Then, comparisons of reactivities and behaviours of these species in GP and AS are analysed.

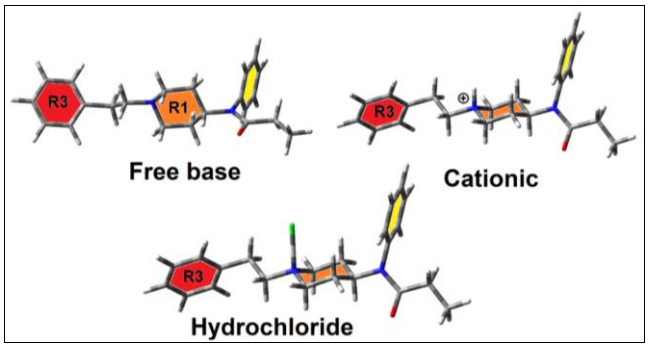

Fig 1: Molecular structures of base, cation and hydrochloride fentanyl

This way, a combined SQMFF and DFT study is very significant to generate safe and consistent assignments of all vibration modes due to the presence of those piperazine, phenylethyl and *N*-phenyl rings in the three species. With that procedure, the vibration modes of three rings are completely assigned despite the couplings of some vibration modes in the lower wavenumber region.

2. Methodology of calculations

The structures of fentanyl species were modelled with the *GaussView* program [26] considering the CIF file published by Ogawa *et al*. [2]. Later, optimizations of species in GP and AS using the B3LYP/6-311++G** method and the Gaussian 16 software were performed [27]. In solution, the IEFPCM method was used in the optimizations [28]. Volumes and variations were obtained using the Moldraw package [29]. Structures of hydrochloride fentanyl species with the descriptions of rings in diverse colours are shown in Fig. 1 while in Fig. 2 are shown the atoms numberings.

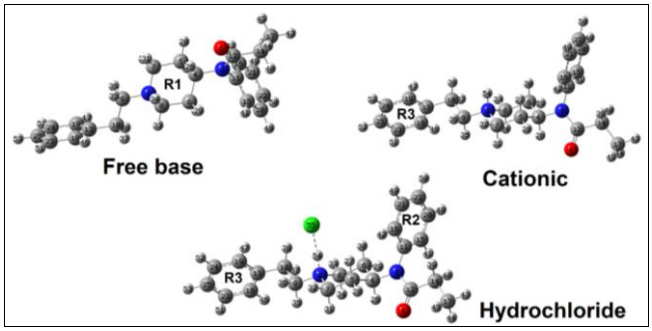

Fig 2: Theoretical structures of base, cation and hydrocloride fentanyl with the atoms numbering and descriptions of rings

The NBO and AIM 2000 packages were combined to predict charges, MEP, bond orders and topological properties, as previously detailed [30-32]. Gap values, frontier orbitals and global descriptors were used [33, 34]. Vibrational assignments were performed using the normal internal coordinates and transferable scaling factors with the harmonic force fields calculated with the SQMFF procedure and the Molvib package [23-25]. Corrections of predicted Raman spectra were performed [35]. The ^{1}H and ^{13}C chemical shifts and the electronic spectra were obtained using respectively the GIAO method [36] and DFT (TD-DFT) calculations with the Gaussian 16 program [27]. Evaluations with theoretical data reported for some comparable species by using the B3LYP/6-31G* method [20, 37] and with experimental IR, Raman, UV and NMR spectra reported for fentanyl [38-42] have been considered in this work.

3. Results and Discussion

3.1 Properties in different media

Table 1 shows the properties obtained for the fentanyl species in GP and AS using the B3LYP/6-311++G** method including solvation energies. Thus, ZPVE energies, dipole moments, volumes and variations volume are revealed in the table. We observed a higher dipole moment of cation in GP and of hydrochloride form in AS while the hydrochloride species shows higher volumes in the two media, as expected due to voluminous Cl atom in its structures.

Table 1: Total energies (*E*), dipole moments (μ), volume variations (ΔV) and solvation energies (ΔG) for the fentanyl species in GP and AS

B3LYP/6-311++G** Method				
Gas phase				
	E_{ZPBE} (Hartrees)	μ (D)	V (Å^3)	
Free Base	-1039.7649	3.39	389.9	
Cation	-1040.1379	5.87	394.4	
Hydrochloride	-1500.6120	5.13	417.4	
PCM				
	E_{ZPBE} (Hartrees)	μ (D)	V (Å^3)	
Free Base	-1039.7836	5.06	391.8	
Cation	-1040.2359	7.93	392.2	
Hydrochloride	-1500.6526	9.42	417.6	
Solvation energy (kJ/mol)				
	$\Delta G_u^{\#}$	ΔG_{ne}	ΔG_c	ΔV (Å^3)
Free Base	-49.0499	21.9868	-71.0367	1.9
Cation	-257.0532	37.3692	-294.4224	-2.2
Hydrochloride	-106.4935	37.0766	-143.5701	0.2

$\Delta G_u^{\#}$. See text

Hence, the terms ΔG_u, ΔG_{ne} and ΔG_c correspond respectively to uncorrected, total non-electrostatic and corrected solvation energies and where, ΔG_u is the difference between E_{ZPBE} in As and GP, ΔG_{ne} is obtained from the PCM calculations and ΔG_c, is the sum of both terms. Regarding the results, the cation shows a higher solvation energy with a substantial volume contraction while the base and hydrochloride forms exhibit slight volume expansions in this medium. The high hydration and solvation energy of cation is justified due to its positive charge while, the increase in μ and volumes of base and hydrochloride are justified by the hydrations with water molecules. Table 2 shows comparisons of solvation energies of three fentanyl species using the B3LYP/6-311++G** and B3LYP/6-31G* methods with those reported for alkaloids using the B3LYP/6-31G* method [20]. Fig. 2 display behaviours of corrected solvation energies (ΔG_c) for the species including fentanyl using the B3LYP/6-31G* method. The rigorous evaluation of table shows that the increase of size basis set is to increase ΔG_c due to increase in E_{ZPVE} and the decreasing of ΔG_{ne}. For instance, for the cation using the B3LYP/6-311++G** method ΔG_{un} = -257.05 kJ/mol and ΔG_{ne} = 37.37 kJ/mol for which the sum ΔG_c = -294.42 kJ/mol while with the lower basis set ΔG_c = -283.11 kJ/mol. In similar form, ΔG_c of base increase from -63.56 to -71.04 kJ/mol.

Table 2: Corrected and uncorrected ΔG by ΔG_{ne} and by ZPVE of three fentanyl species using the B3LYP/6-31G* method compared with other alkaloids

Solvation energy (kJ/mol)			
Condition	$\Delta G_{un}^{\#}$	ΔG_{ne}	ΔG_c
Free base			
Fentanyl[a]	-40.28	23.28	-63.56
Morphine[b]	-47.74	13.17	-60.91
Cocaine[c]	-42.75	28.51	-71.26
Scopolamine[d]	-56.66	18.81	-75.47
Heroin[e]	-59.54	29.13	-88.67
Cationic			
Fentanyl[a]	-245.32	37.79	-283.11
Morphine[b]	-282.23	26.96	-309.19
Cocaine[b]	-216.66	38.58	-255.24
Scopolamine[b]	-279.87	30.47	-310.34
Heroin[b]	-280.13	43.01	-323.14
Hydrochloride			
Fentanyl[a]	-94.58	37.03	-131.61
Morphine[b]	-118.82	25.92	-144.74
Cocaine[b]	-99.94	38.20	-138.14
Scopolamine[b]	-95.19	27.55	-122.74
Heroin[b]	-118.56	43.38	-161.94
Fentanyl[a]			
B3LYP/6-311++G** method			
Free Base	-49.05	21.99	-71.04
Cation	-257.05	37.37	-294.42
Hydrochloride	-106.49	37.08	-143.57

[a]This work, [b]From Ref [20].

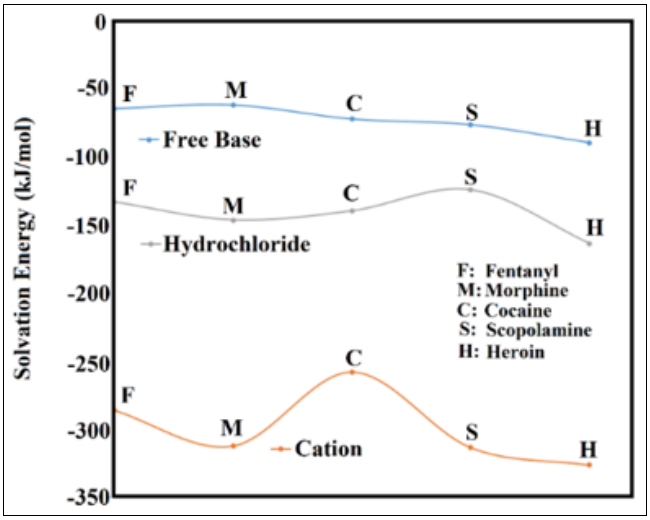

Fig 3: Corrected ΔG of base, cationic and hydrocloride fentanyl compared with other species by using the B3LYP/6-31G* method

The hydrochloride species increase from -131.61 to -143.57 kJ/mol when the higher basis set is used. Then, Fig. 2 shows that the cations of all the alkaloids have the most negative solvation energies, ΔG_c, where cocaine presents the less negative value (-255.24 kJ/mol). Here, the three species of heroin show values that are more negative. Previous studies have demonstrated that the hydrochloride forms in solution and in solid phase are as cations, probably because these species show higher solubility and, for this reason, they are very used in pharmaceutical preparations. In this study, ΔG_c of fentanyl base with the B3LYP/6-311++G** method (-71.04 kJ/mol) is approximately similar to cocaine (-71.26 kJ/mol) while the values of cation (-294.42 kJ/mol) and hydrochloride (-143.57 kJ/mol) are comparable respectively to observed for morphine (-309.19 and -144.74 kJ/mol).

3.2 Geometrical parameters

Relationships among experimental and optimized parameters of three fentanyl species are important to perform reliable vibrational analyses [2]. Hence, Table 2 shows comparisons of parameters of base, cation and hydrochloride fentanyl in GP and AS with the corresponding experimental for the base [2]. The concordances between the structures are shown using the RMSD.

Table 2: Calculated parameters of base, cation and hydrochloride fentanyl in GP and AS related with the experimental for the base

Parameters	0						
	Free Base		Cation		Hydrochloride		Exp.[b]
	Gas	PCM	Gas	PCM	Gas	PCM	
Bond lengths (Å)							
N2-C7	1.465	1.473	1.519	1.511	1.499	1.508	1.460
N2-C8	1.464	1.473	1.517	1.511	1.496	1.507	1.461
N2-C9	1.463	1.471	1.521	1.511	1.498	1.508	1.477
C9-C10	1.540	1.538	1.532	1.531	1.536	1.532	1.486
C10-C13	1.512	1.513	1.517	1.514	1.515	1.514	1.522
C4-C6	1.533	1.532	1.534	1.535	1.531	1.530	1.517
C4-C5	1.534	1.532	1.539	1.532	1.537	1.535	1.519
C4-N3	1.483	1.488	1.466	1.482	1.480	1.485	1.480
N3-C11	1.437	1.443	1.441	1.444	1.439	1.444	1.440
N3-C12	1.386	1.365	1.399	1.368	1.384	1.366	1.368
C12=O	1.223	1.243	1.220	1.241	1.224	1.242	1.223
C12-C14	1.528	1.522	1.520	1.521	1.526	1.521	1.517
C14-C17	1.527	1.525	1.527	1.526	1.527	1.525	1.465
C13-C19	1.400	1.401	1.398	1.400	1.400	1.400	1.370
C19-C24	1.394	1.395	1.393	1.395	1.393	1.395	1.374
C24-C25	1.394	1.396	1.394	1.395	1.394	1.395	1.377
C25-C23	1.394	1.395	1.394	1.395	1.393	1.395	1.364
C23-C18	1.394	1.396	1.393	1.395	1.394	1.395	1.395
C18-C13	1.400	1.401	1.398	1.400	1.398	1.400	1.395
C8-C6	1.531	1.530	1.526	1.524	1.529	1.526	1.526
C5-C7	1.531	1.529	1.524	1.523	1.526	1.523	1.524
C11-C15	1.398	1.397	1.398	1.397	1.398	1.396	1.377
C15-C20	1.393	1.394	1.393	1.394	1.393	1.394	1.381
C20-C22	1.394	1.395	1.394	1.395	1.394	1.395	1.369
C22-C21	1.394	1.395	1.394	1.395	1.393	1.395	1.355
C21-C16	1.394	1.394	1.394	1.394	1.393	1.395	1.385
C16-C11	1.398	1.397	1.398	1.397	1.397	1.397	1.377
RMSD	**0.02**	**0.02**	**0.03**	**0.03**	**0.02**	**0.03**	
Bond angles (º)							
C13-C10-C9	112.0	111.5	110.0	110.4	110.5	110.1	117.0
C10-C9-N2	113.4	114.2	113.8	113.0	113.7	114.0	111.8
C9-N2-C8	112.9	111.1	113.4	113.0	113.8	112.8	111.1
N2-C8-C6	111.4	112.2	111.4	111.2	111.5	111.9	110.1
C8-C6-C4	110.5	110.3	111.1	111.1	110.7	110.7	109.4
C6-C4-C5	109.8	109.9	109.7	109.6	109.5	109.3	110.1
C6-C4-N3	113.1	113.0	113.3	112.6	113.0	112.9	112.3
C4-C5-C7	110.4	110.2	111.3	110.5	110.9	110.9	109.9
C5-C7-N2	111.3	112.1	111.2	111.3	111.2	111.9	111.9
C4-N3-C12	118.5	119.9	116.6	119.1	116.8	118.7	118.1
C4-N3-C11	119.4	118.8	120.2	119.2	120.4	119.4	119.2
N3-C12-O1	121.8	121.8	120.3	121.5	120.9	117.5	121.4
N3-C12-C14	116.8	117.5	116.9	117.4	117.2	117.5	117.3
C12-C14-C17	112.5	113.4	112.6	113.4	112.5	113.5	113.5
RMSD	**1.62**	**1.80**	**2.27**	**1.98**	**2.13**	**2.36**	
Dihedral angles (º)							
C13-C10-C9-N2	-175.5	-179.5	-173.9	-173.5	-167.4	-174.9	-169.1
C10-C9-N2-C8	-73.6	-73.7	-66.7	-68.2	-61.1	-62.6	-76.4
C7-N2-C8-C6	-59.7	-59.2	-56.4	-56.3	-56.5	-55.1	-62.5
C6-C4-C5-C7	53.7	53.9	55.9	56.6	56.3	56.8	53.5
C5-C4-N3-C12	113.5	-118.3	98.6	135.3	82.9	88.4	88.8
C4-N3-C12-O1	0.1	0.8	0.5	-1.2	1.7	2.3	-
C4-N3-C12-C14	-180.0	-179.2	-179.7	-179.3	-178.1	-178.1	-

N3-C12-C14-C17	-179.4	-178.5	-175.7	-175.0	174.8	-177.4	154.1
C11-N3-C12-O1	179.4	179.5	174.2	-175.0	178.1	175.3	-172.4
C16- C11-N3-C12	-89.5	-88.9	-85.8	-95.0	-97.8	-88.1	-79.9
RMSD	**161.85**	**175.61**	**159.58**	**110.34**	**117.34**	**160.26**	

[a]This work. [b]Ref [2]

Here, very good concordances show the theoretical parameters using the hybrid B3LYP/6-311++G** method with discrepancies in bond lengths among 0.03 and 0.02 Å and in bond angles among 2.4 and 1.6 º. Higher RMSD differences show the dihedral angles (175.6-117.3 º) due to the changes in the signs of N3-C12-C14-C17, N3-C12-C14-C17 and C11-N3-C12-O1 angles. Hence, such changes justify the high differences in the RMSDs. Here, the protonation of N2 has little influence on the parameters, as also was observed for fentanyl and its analogue N-(1-Phenylpyrazol-3-yl)-N-[1-(2-phenylethyl) 4-piperidyl]propanamide [42].

3.3 Charges, electrostatic potentials and bond orders

Mulliken, MK and NPA charges, MEP and bond orders studies (BOs) were studied to describe the electronic distributions in the entire surfaces of species. Therefore, the results for the fentanyl species using the hybrid B3LYP/6-311++G** method are shown in Tables S1, S2 and S3 (Supporting Material) while Figs. 4a and 4b show the variations of charges on the N2, N3 and O1 atoms of base in the two media. These atoms are important because they are donor of H bonds. In relation to figures, the three charges on N2, N3 and O1 of base show almost identical variations in both media with positive Mulliken charges on N2 and N3 while on O1 are predicted negative charges. Then, MK and NPA charges on the three atoms of base show negative signs with similar behaviours in both media and, where the MK charges on N2 display higher values than N3. In the cation, those three charges on the three atoms reveal the same behaviours but only the MK charges on N2 show positive signs, as expected because these atoms are positively charged in this species while the Mulliken and NPA charges on these atoms show negative signs. When the charges are analysed in the hydrochloride form, the MK and Mulliken charges show positive signs in both media revealing nearly similar values in solution while the NPA charges show few variations in both media and negative signs on the N and O atoms. From Tables S1, S2 and S3, the NPA charges on H54 linked to N2 in the cation reveal high values (0.407/0.405 a.u.) while the Mulliken and MK charges decrease from the GP (0.342/0.341 a.u.) to solution (0.291/0.286 a.u.). In the hydrochloride species low charges values are predicted on H54 diminishing in solution.

Evaluating MEPs for fentanyl species in both media from Table S4, we observed few variations among the species and, only the classical tendency due to the electronegativities are detected. Thus, MEP Cl > O > N > C > H whereas the graphs of MEP surfaces of three fentanyl species in GP are shown in Fig. 5. Similar models are obtained in solution and, for this reason, they are not presented here. However, the energies MEPs of species show changes in AS. For instance, the free base increases from ±0.060 a.u. in GP to ±0.063 a.u. in solution; the cation increases from ±0.190 to 0.229 a.u and, the hydrochloride species from ±0.067 to 0.080 a.u., being the cation the species that experiences the greatest variation in water. Then, the different colorations of MEP surfaces reveal a strong red colour on O1 of free base with slight blue colours on the H atoms of rings while the entire surface of cation revels blue colours, as expected due to the positive charge. The hydrochloride species shows intense red colour on Cl with a slight orange colour on O1.

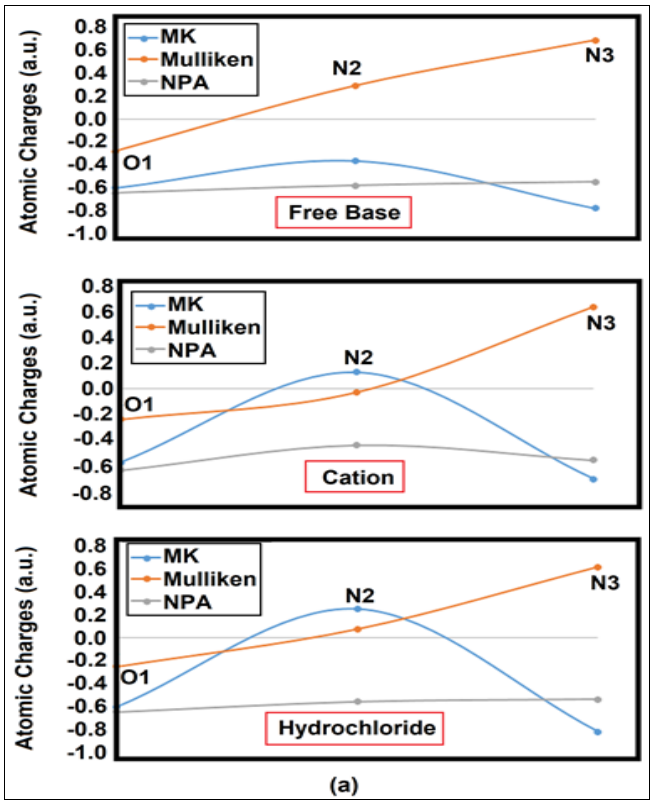

Fig 4a: MK, Mulliken and NPA charges on O1, N2, and N3 atoms of fentanyl base in GP using the B3LYP/6-311++G** method

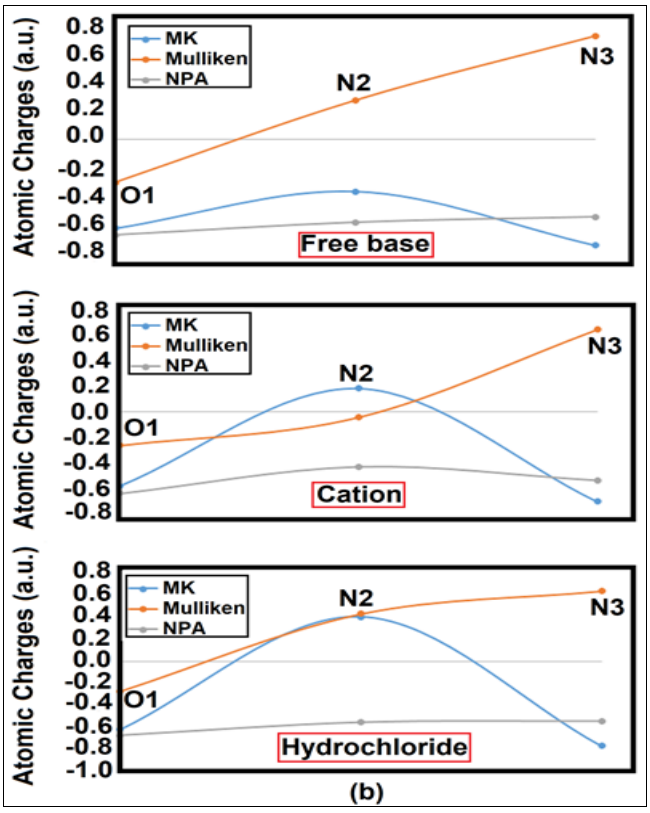

Fig 4b: MK, Mulliken and NPA charges on O1, N2, and N3 atoms of fentanyl base in AS using the B3LYP/6-311++G** method

Hence, the red, blue and green colours are associated respectively to nucleophilic, electrophilic and inert regions. The intense red colour on Cl atom in hydrochloride species is justified by its electronegativity while the less negative values on the H54 of cation and hydrochloride species indicate that these atoms are the more labile H atoms. The different colorations evidently expose the places reacting with potential biological nucleophiles or electrophiles reactive.

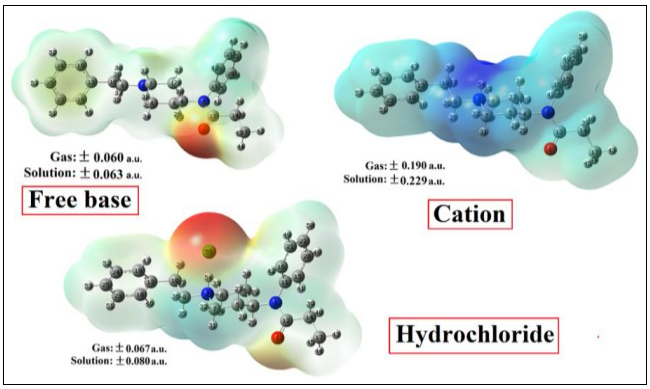

Fig 5: Calculated MEP surfaces of base, cation and hydrocloride fentanyl in both media using the B3LYP/6-311++G** method

Regarding bond orders (BO), from Table S5, we observed decreasing in BO values of O1 in the three species and of N2 of base from the GP to solution while the BOs of N2 in the cation and hydrochloride slightly increase in solution. These changes are associated to N2-H54 bonds of cation and hydrochloride species. Then, the BOs of N3 increase from the GP to solution in the three species. The hydration of O1 and N3 with water molecules justify these changes because these sites are donors H bonds, as exposed by MEP surfaces.

3.4 Natural Bond Orbital (NBO) study

The donor H bonds atoms and different *N*-phenyl, phenyl-ethyl and piperidin rings in the structures of three fentanyl species confer the potent opioid analgesic properties of these species and, hence, the stabilization energies are predicted then analysed in this section by using NBO calculations [30]. Thus, Table S6 shows the donor-acceptor energy interactions of base and hydrochloride fentanyl species in both media by using the B3LYP/6-311++G** level of theory. The rigorous evaluation of table reveal only three interactions for the base in the two media, which are, the $\pi \rightarrow \pi^*$, $n \rightarrow \pi^*$ and $n \rightarrow \sigma^*$ interactions while the cation shows four $\pi \rightarrow \pi^*$, $n \rightarrow \pi^*$, $n \rightarrow \sigma^*$ and $\pi^* \rightarrow \pi^*$interactions. On the other side, in the hydrochloride species are predicted in both media the five $\pi \rightarrow \pi^*$, $n \rightarrow \sigma^*$, $n \rightarrow \pi^*$, $\sigma \rightarrow n^*$ and $n \rightarrow n^*$. The estimations of energies show that the $\pi \rightarrow \pi^*$ transitions are energetically strong in the base while in the cation the $\pi^* \rightarrow \pi^*$ interactions. In the hydrochloride, the most energetically strong interactions are observed in the $n \rightarrow n^*$ transitions. Analysing total energies, the base shows low values in both media (1469.5/1474.15 kJ/mol) then, the cation (1690.78/1775.90 kJ/mol) and, the higher energies are observed in the hydrochloride species (3458.82/3372.54 kJ/mol). Hence, these NBO calculations show that the hydrochloride fentanyl shows the greater electronic stability in both media while the base and the cation are the less stable species.

3.5 Atoms in Molecules (AIM) studies

The topological properties can predict different interactions, as suggested by the Bader's AIM theory [31]. Hence, for the three fentanyl species, the electron density, $\rho(r)$, the Laplacian values, $\nabla^2\rho(r)$, the eigenvalues $(\lambda 1, \lambda 2, \lambda 3)$ of the Hessian matrix and, the $|\lambda 1|/\lambda 3$ ratio were calculated in BCPs and RCPs using the B3LYP/6-311++G** method [32]. Therefore, Table S7 show the properties while the molecular graphs are revealed in Fig 6 and 7. The base and cation in both media show two new H bonds interactions, which are C10-H37···H33-C8 and C12-O1···H26-C4 with two new RCPN1 and RCPN2. The hydrochloride species in GP and AS shows four C10-H38···Cl55, N2-H54···Cl 55, C5-H27···Cl55 and C5-H27···H42-C16 interactions and, where C5-H27···Cl55 disappears in solution forming a new C10-H37···H33-C8 interaction, as shown in Fig. S1. These interactions show that $\lambda 1/\lambda 3 < 1$ and $\nabla^2\rho(r) > 0$, for which, the interaction is of H bonds or ionic. Distances between the two involved atoms are shown in Table S7. A very significant resulted observed in the hydrochloride form in GP is that the density of N2-H54···Cl55 interaction decrease in AS while $\nabla^2\rho(r)$ increase and the λ values decrease.

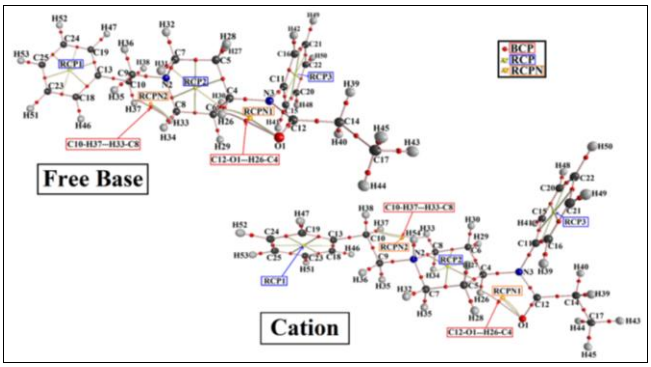

Fig 6: Molecular graphs for the base and cation of fentanyl in GP phase viewing the BCPs and RCPs using the B3LYP/6-311++G** method

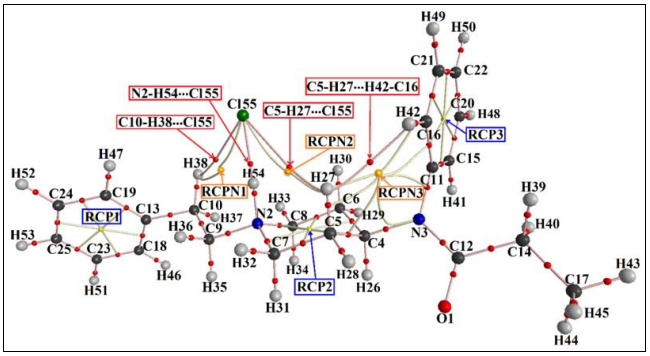

Fig 7: Molecular graph for hydrochloride fentanyl in GP showing the BCPs and RCPs using the B3LYP/6-311++G** method

3.6 Frontier orbitals and quantum global descriptors

Reactivities and behaviours of three fentanyl species in both media were predicted with the frontier orbitals by using the gap values and the hybrid B3LYP/6-311++G** method, according to Parr and Pearson [33, 34]. These parameters are important since the interesting medicinal and pharmacological properties of fentanyl [1-19]. Later, the chemical potential (μ), electronegativity (χ), global hardness (η), global softness (S), global electrophilicity index (ω) and

global nucleophilicity index (□) descriptors were computed from known equations [20, 37-39]. The results of these factors and the equations used are shown in Table 3. Small energy gap specifies > chemical reactivity and < kinetic stability because this latter factor is related to the difference HOMO-LUMO energy (GAP). Hence, the hydrochloride form in solution shows the lower gap value (4.4545 eV) and, therefore, this species is the most reactive one whereas the cation in GP is the less reactive (5.4940 eV). Probably, the > stabilization energy of hydrochloride in solution justify its low kinetic stability, as reinforced by NBO calculations.

Table 3 Calculated frontier orbitals, gap, chemical potential (μ), electronegativity (χ), global hardness (η), global softness (S), global electrophilicity index (ω) and global nucleophilicity index (□) for base, cation and hydrochloride species of fentanyl using the hybrid B3LYP/6-311++G** level of theory

Frontier orbitals (eV)	Free Base		Cation		Hydrochloride	
	Gas	PCM	Gas	PCM	Gas	PCM
HOMO	-6.0817	-6.2178	-9.4913	-9.3852	-6.1851	-5.5375
LUMO	-0.9524	-0.9850	-3.9973	-4.0708	-0.9714	-1.0830
GAP	5.1293	5.2327	5.4940	5.3144	5.2137	4.4545
Descriptors (eV)						
□	3.5171	3.6014	6.7443	6.7280	3.5783	3.3103
□	-3.5171	-3.6014	-6.7443	-6.7280	-3.5783	-3.3103
□	3.0409	3.1089	4.7457	4.6926	3.0926	2.7687
S	0.1644	0.1608	0.1054	0.1066	0.1617	0.1806
□	2.0339	2.0860	4.7924	4.8231	2.0701	1.9788
□	-1.1566	-1.1584	-1.4212	-1.4337	-1.1571	-1.1956

□ = - [E(LUMO) + E(HOMO)]/2;□□ = [E(LUMO) + E(HOMO)]/2; □ = [E(LUMO) – E(HOMO)]/2;
S = ½□□□ = □²/2□□□□□□□□□

The base evidence < gap than the cation in both media. Gap values for fentanyl species by using the B3LYP/6-31G* method are related in Table 4 with reported for morphine, cocaine, scopolamine and heroin at the same level of theory [20]. Thus, we detected that the base and hydrochloride species of cocaine in both media show < gaps and > reactivities while the cation of morphine in GP is the most reactive. Previously, we see that ΔG_c of free base of fentanyl with the B3LYP/6-311++G** level of theory (-71.04 kJ/mol) is approximately similar to cocaine (-71.26 kJ/mol) while the values of cation (-294.42 kJ/mol) is similar to morphine (-309.19 and -144.74 kJ/mol). Examining the descriptors predicted from Table 3, the cationic species in both media present the highest global electrophilicity and nucleophilicity indexes than the other ones, a result similar to observed for both enantiomers of promethazine [37].

Table 4: Gap values for the fentanyl species related to other species in GP and AS by using the B3LYP/6-31G* level of theory

Orbital	Fentanyl[a]	Scopolamine[#,b]	Heroin[b]	Morphine[b]	Cocaine[b]
Free base/GAS					
GAP	5.3367	5.4004	5.6563	5.6044	4.8580
Free base/Aqueous solution					
GAP	5.4297	5.4758	5.6414	5.4750	4.9487
Cationic/Gas phase					
GAP	6.1843	5.6356	5.4268	5.1889	5.4468
Hydrochloride/Gas phase					
GAP	5.2947	4.9239	5.3024	5.4417	3.6813
Hydrochloride/Aqueous solution					
GAP	4.5533	5.4026	4.4469	4.5840	3.6813

[#]Hydrobromide, [a]This work, [b]From Ref [20]

3.7 Vibrational study

The three fentanyl species were optimized with C_1 symmetry by B3LYP/6-311++G** calculations and, due to the 50, 51 and 52 atoms in the structures are expected respectively 153, 156 and 159 normal vibration modes for base, cation and hydrochloride. The experimental IR and Raman spectra of hydrochloride fentanyl in the solid state are observed in Figs. 8 and 9 respectively related to the predicted for the three species in GP. Besides, the experimental IR spectrum of base was also related to the predicted for the three species in GP in Fig. S2. The experimental spectra are available from Ref. [38] and, in particular, the theoretical Raman spectra were transformed to intensities [35]. Very good correlations show the compared spectra for the free base (Fig. S2). However, we can see from Figs. 8 and 9 an important difference between the experimental and predicted spectra for hydrochloride because the strong IR band predicted by calculations at 1994 cm^{-1} and, that in the Raman spectrum is observed with lower intensity, is not observed in the experimental spectra. Such differences occur because in the solid and in solution the hydrochloride species are as cationic ones, as also was observed in other hydrochloride compounds. Then, the cation shows the best correlations, in particular in solution while the base in this medium is protonated forming the cation.

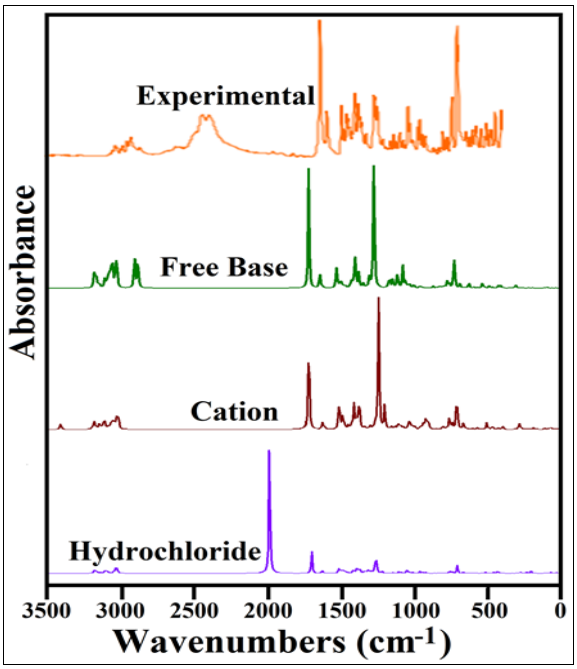

Fig 9: Experimental infrared spectrum of hydrochloride fentanyl in the solid state [38] compared with the predicted for base, cation and hydrochloride using the B3LYP/6-311++G** method

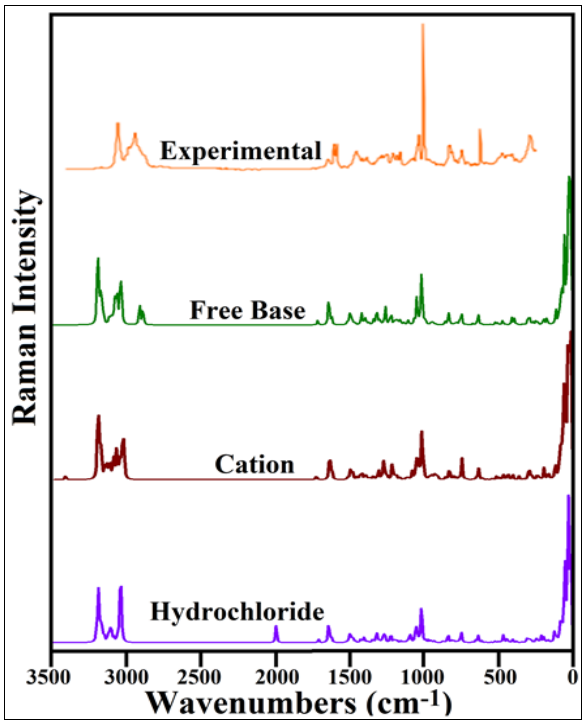

Fig 10: Experimental Raman spectrum of hydrochloride fentanyl in the solid state [38] compared with the predicted for base, cation and hydrochloride using the B3LYP/6-311++G** method

The vibrational assignments were carried out by using the harmonic force fields [23-25]. Here, PED contributions ≥ 10% were considered. Table 5 shows observed and calculated wavenumbers and assignments for the three species of fentanyl in GP. Then, deliberations of some assignments by sections are shown below.

3.7.1 Bands Assignments

3.7.1.1 4000-2000 cm^{-1} range. The anti-symmetric and symmetric modes of νCH_2 and νCH_3 groups of three forms of fentanyl are expected together with the νC-H stretching modes and the νN2-H54 of cationic and hydrochloride species. The very weak IR band at 3369 cm^{-1} is assigned to νN2-H54 of cation, as predicted by calculations while in the hydrochloride form this mode is predicted at 1913 cm^{-1} because the N2-H54 bond is linked to Cl55 and, thus, the band is shifted at < wavenumbers. The aromatic νC-H vibrations of two rings of fentanyl species are assigned among 3067 and 3018 cm^{-1}, as predicted by SQM calculations while the aliphatic νC-H vibrations are assigned between 2983 and 2917 cm^{-1} [20, 37]. The anti-symmetric and symmetric stretching modes of νCH_2 and νCH_3 groups are assigned around 3021 and 2763 cm^{-1}, as detailed in Table 5 [20, 37].

Table 5: Observed and calculated wavenumbers (cm^{-1}) and assignments for the three fentanyl species in GP by using the B3LYP/6-311++G** method

Experimental[c]		B3LYP/6-311++G** Method[a]					
IR	Raman	Free base		Cationic		Hydrochloride	
		SQM[b]	Assignments[a]	SQM[b]	Assignments[a]	SQM[b]	Assignments[a]
3369vw				3258	νN2-H54		
		3062	νC22-H50, νC15-H41	3065	νC22-H50,νC21-H49	3067	νC16-H42
		3057	νC15-H41,νC16-H42	3061	νC25-H53		
	3055 s	3055	νC25-H53	3060	νC16-H42,νC15-H41	3058	νC22-H50
				3055	νC22-H50	3057	νC25-H53
		3051	νC22-H50	3050	νC23-H51	3051	νC21-H49
3042vw		3044	νC24-H52,νC23-H51	3046	νC21-H49,νC20-H48	3046	νC23-H51,νC24-H52
		3041	νC21-H49	3042	νC24-H52	3043	νC15-H41
		3035	νC25-H53, νC18-H46	3040	νC22-H50,νC20-H48	3037	νC25-H53,νC19-H47
		3033	νC20-H48	3027	νC18-H46	3034	νC20-H48
		3023	νC18-H46	3025	νC19-H47	3028	νC19-H47
2994vw		3021	νC19-H47	3021	ν_aCH_2(C8)	3018	νC18-H46
				3012	ν_aCH_2(C9)	2997	ν_aCH_2(C8)
	2985 m			3006	ν_aCH_2(C7)	2986	ν_aCH_3
		2987	ν_aCH_3	2984	ν_aCH_3	2983	ν_aCH_2(C7),ν_aCH_2(C9)
				2983	νC4-H26	2979	ν_aCH_2(C5)
		2975	ν_aCH_3	2973	ν_aCH_3	2976	ν_aCH_2(C5), ν_aCH_2(C7)
				2971	ν_aCH_2(C5), ν_aCH_2(C6)	2975	ν_aCH_3
		2964	νC4-H26	2966	νC4-H26,ν_aCH_2(C5)	2968	ν_aCH_2(C6)
2954 w		2958	ν_aCH_2(C10)	2965	ν_aCH_2(C10)	2956	ν_aCH_2(C10)
		2948	ν_aCH_2(C8)	2956	ν_sCH_2(C9)		
		2946	ν_aCH_2(C5)	2953	ν_sCH_2(C8)		
	2942 s	2940	ν_aCH_2(C6)	2948	ν_sCH_2(C7)		
		2936	ν_aCH_2(C14)	2945	ν_aCH_2(C14)	2937	ν_aCH_2(C14)
2930 w		2933	ν_aCH_2(C7)			2930	ν_sCH_2(C5)
	2923 m	2925	ν_aCH_2(C9)	2918	ν_sCH_2(C6)	2921	ν_sCH_2(C6)
		2914	ν_sCH_3	2916	ν_sCH_2(C5)	2918	ν_sCH_2(C9)
		2913	ν_sCH_2(C10)	2916	ν_sCH_2(C14)	2917	νC4-H26
		2910	ν_sCH_2(C14)	2914	ν_sCH_3	2915	ν_sCH_3
	2880 sh	2905	ν_sCH_2(C6)	2909	ν_sCH_2(C10)	2912	ν_sCH_2(C10)
2869vw		2903	ν_sCH_2(C5)			2910	ν_sCH_2(C14)
		2790	ν_sCH_2(C9)			2906	ν_sCH_2(C7)
2445 m		2770	ν_sCH_2(C7)			2901	ν_sCH_2(C8)
2397 m		2763	ν_sCH_2(C8)				
						1913	νN2-H54
1646 vs	1651 w	1653	νC12=O1	1584	νC12=O1, νC16-C21	1648	νC12=O1
1598 m	1608 m	1590	νC18-C23,νC19-C24	1584	νC19-C24,νC18-C23	1590	νC19-C24, νC18-C23
	1589 m	1582	νC15-C20,νC16-C21	1568	νC20-C22,,νC21-C22	1582	νC15-C20νC16-C21
		1569	νC23-C25, νC24-C25, νC13-C18,νC13-C19	1567	νC23-C25,νC24-C25, νC13-C18,νC13-C19	1570	νC23-C25,νC24-C25, νC13-C18,νC13-C19
	1537vw	1567	νC21-C22, νC20-C22	1565	νC12=O1	1568	νC20-C22,νC21-C22
						1486	ρ'N2-H54,τ_wN2-H54
1494 s		1479	βC23-H51,βC24-H52	1479	βC24-H52,βC23-H51	1480	βC23-H51,βC24-H52
1477 w		1478	βC20-H48,βC21-H49	1477	βC20-H48,βC21-H49	1479	βC21-H49,βC20-H48
						1473	ρN2-H54
1461 m	1462 m	1451	δCH_2(C7)	1454	δCH_2(C7),δCH_2(C9)	1443	δCH_2(C10)
1441 m		1439	βC25-H53, βC23-H51	1441	βC25-H53,βC23-H51	1440	βC25-H53
		1439	δ_aCH_3	1440	δ_aCH_3	1439	δ_aCH_3
1437 w		1437	δCH_2(C10)	1436	βC22-H50,βC21-H49	1436	δCH_2(C10), δCH_2(C8)
		1434	βC22-H50,βC21-H49	1435	δCH_2(C8),δCH_2(C9)	1435	βC22-H50,βC20-H48
		1434	δCH_2(C8)	1433	δ_aCH_3	1431	δCH_2(C7)
		1429	δCH_2(C5)	1431	δCH_2(C6)	1428	δ_aCH_3
		1428	δ_aCH_3	1428	δCH_2(C7)	1428	δCH_2(C8), δCH_2(C6)
		1423	δCH_2(C9)	1423	δCH_2(C5)	1419	δCH_2(C9)
	1414 w	1415	δCH_2(C6)	1417	δCH_2(C10)	1414	δCH_2(C5)
		1402	wagCH_2(C7)	1405	wagCH_2(C7)	1401	wagCH_2(C9)
1406 s	1395 w	1398	δCH_2(C14)	1396	ρN2-H54, wagCH_2(C9)	1397	δCH_2(C14)
		1389	ρ'C4-H26,wagCH_2(C9)	1390	δCH_2(C14)	1394	ρ'C4-H26
1381 s		1382	wagCH_2(C8)	1387	ρ'N2-H54	1381	wagCH_2(C8)
				1384	νN3-C12,wagCH_2(C14)	1372	wagCH_2(C6)
		1365	wagCH_2(C14), wagCH_2(C6)	1379	wagCH_2(C6),wagCH_2(C5)	1362	wagCH_2(C6), wagCH_2(C14)

1365 m		1358	ρC4-H26	1371	wagCH$_2$(C8)	1357	wagCH$_2$(C7)
		1354	δ$_s$CH$_3$	1364	δ$_s$CH$_3$	1354	δ$_s$CH$_3$
1345 s				1360	ρC4-H26	1352	wagCH$_2$(C14)
		1351	wagCH$_2$(C7),wagCH$_2$(C8)	1348	wagCH$_2$(C7), wagCH$_2$(C10)	1332	βC18-H46,βC19-H47
		1345	wagCH$_2$(C14),wagCH$_2$(C5)	1346	ρ'C4-H26		
1325 w		1327	βC18-H46, βC19-H47	1331	βC18-H46,βC19-H47	1320	wagCH$_2$(C10) wagCH$_2$(C5), ρC4-H26
		1316	wagCH$_2$(C5)	1317	wagCH$_2$(C5),ρC4-H26	1313	wagCH$_2$(C10), ρC4-H26
		1309	βC15-H41,βC16-H42	1310	βC15-H41,ρCH$_2$(C9)		
		1304	ρCH$_2$(C9)	1308	βC16-H42,βC15-H41	1310	βC16-H42,βC15-H41
	1296 m	1296	wagCH$_2$(C10)	1297	wagCH$_2$(C10)	1301	wagCH$_2$(C10)
		1287	ρCH$_2$(C8)	1292	νC19-C24,νC18-C23	1288	ρCH$_2$(C8)
		1281	ρCH$_2$(C9)	1274	ρCH$_2$(C6)	1279	ρCH$_2$(C6),ρCH$_2$(C9)
1277 s		1266	νC11-C16,νC11-C15	1270	νC11-C16,νC11-C15	1269	νC11-C16,νC11-C15
1261 s	1258 m	1261	ρCH$_2$(C5), ρCH$_2$(C6)	1261	νN3-C12, wagCH$_2$(C14)	1260	ρCH$_2$(C5), ρCH$_2$(C6)
		1254	ρCH$_2$(C14)	1260	ρCH$_2$(C14)	1253	ρCH$_2$(C14)
1245 m		1236	ρCH$_2$(C7)	1242	ρCH$_2$(C5)	1239	νN3-C12
1236 sh		1233	νN3-C12, ρC12=O1	1231	ρCH$_2$(C7), ρCH$_2$(C8)	1237	ρCH$_2$(C7)
	1221 m	1220	νN3-C11	1210	νN3-C11	1226	νN3-C11
1209 w		1191	νC10-C13	1185	νC10-C13	1187	νC10-C13
	1188 w	1185	ρCH$_2$(C10)	1174	ρCH$_2$(C10),ρCH$_2$(C9)	1182	ρCH$_2$(C10)
1168 w	1164 m	1168	βC23-H51,βC24-H52	1171	βC23-H51,βC24-H52	1169	βC24-H52
		1160	βC21-H49,βC20-H48	1161	βC16-H42,βC15-H41, βC21-H49	1162	βC21-H49
		1152	ρCH$_2$(C10), ρCH$_2$(C6)	1153	βC22-H50,βC20-H48	1156	ρCH$_2$(C5)
1136 w		1149	βC22-H50	1153	βC25-H53	1149	βC23-H51
		1147	βC25-H53	1131	ρCH$_2$(C6),ρCH$_2$(C5)	1149	βC22-H50,βC20-H48
1121vw		1122	νN2-C8				
1100 w		1112	νN2-C9,νN2-C7			1099	νC4-C6
1080 w	1083 w			1088	τR$_1$(A1)	1084	νN3-C4, ρCH$_3$
		1079	ρCH$_3$,νC14-C17	1081	νC4-C5,νC4-C6	1079	τR$_1$(A1)
		1070	νC4-C6	1078	ρCH$_3$,νC14-C17	1065	νN2-C9
		1067	νC4-C5	1066	νC18-C23,νC19-C24	1063	νC16-C21,νC15-C20
		1061	νC15-C20,νC16-C21	1063	νC15-C20,νC16-C21	1059	νN2-C9
		1058	τR$_1$(A1)	1056	ρ'CH$_3$	1048	ρ'CH$_3$
1040 s	1046 s	1047	ρ'CH$_3$	1050	βR$_1$(A1), νN3-C4	1045	νN2-C8
		1034	νN3-C4	1023	νC9-C10	1026	νC9-C10,νN2-C9
1024 m		1020	βR$_1$(A3)	1020	βR$_1$(A3)	1020	βR$_1$(A3)
	1018 vs	1018	βR$_1$(A2)	1017	βR$_1$(A2)	1019	νC5-C7,νC9-C10
		1016	νC9-C10	1012	γC22-H50	1018	βR$_1$(A2)
		1000	γC22-H50	1009	γC25-H53	1000	γC22-H50
1008 w				1009	νC5-C7		
				1006	νC6-C8		
		998	βR$_1$(A2), νC20-C22	997	βR$_1$(A2),νC12-C14	998	βR$_1$(A2), νC20-C22
		995	βR$_1$(A3), νC23-C25	993	βR$_1$(A3),νC23-C25	995	βR$_1$(A3),νC24-C25
		990	γC25-H53	992	νC6-C8,νC5-C7	995	γC24-H52, γC25-H53
		989	νC6-C8,ρCH$_3$	988	γC20-H48,γC21-H49	993	νC6-C8
980 w		982	γC15-H41, γC21-H49	980	γC24-H52,γC23-H51	979	γC20-H48
	979 w	979	νC6-C8	969	νN2-C9, νC6-C8	977	γC23-H51
		972	γC23-H51, γC24-H52	955	τwCH$_2$(C9)	975	νC14-C17
963 m		962	νC5-C7			955	τwCH$_2$(C9), τwCH$_2$(C10)
	945 w	944	βR$_1$(A1)			946	νC9-C10
935 w		934	γC16-H42,γC15-H41	938	γC15-H41	932	γC15-H41,γC16-H42
918 w		929	τwCH$_2$(C9)	927	νC9-C10	923	γC18-H46,γC19-H47
912 vw		910	γC18-H46,γC19-H47	920	γC18-H46,γC19-H47	906	νN2-C7
	908 vw	909	νC14-C17	899	νN2-C8	903	τwCH$_2$(C6)
				889	νN2-C9,νN2-C7		
863 vw		880	τwCH$_2$(C7), τwCH$_2$(C8)	857	τwCH$_2$(C8),τwCH$_2$(C7)	868	τwCH$_2$(C7), τwCH$_2$(C8)
		847	γC16-H42,γC20-H48, γC21-H49,γC15-H41	851	γC16-H42	849	γC18-H46,γC19-H47
		845	γC18-H46,γC19-H47, γC23-H51,γC24-H52	844	γC19-H47,γC18-H46	843	γC15-H41,γC16-H42, γC21-H49
827 vw	837 m	832	νN2-C8	833	νN2-C8	837	νN2-C8,νC4-C5
807 w	818 m	806	νC4-C6,νC4-C5	807	νC10-C13	810	νC10-C13
	790 w	783	γN3-C11	789	τR$_1$(A2),γC22-H50	786	τR$_1$(A2),γC22-H50
775 w		776	γC12=O1, τwCH$_2$(C14)	786	γC12=O1	777	γC12=O1

		758	τR_1(A3),γC25-H53	758	τR_1(A3),γC25-H53	756	νN2-C7
	752 m	751	τwCH_2(C5),τwCH_2(C6)	750	νN2-C7,νN2-C8	754	τR_1(A3),γC25-H53
	752 m	746	τR_1(A3), γC25-H53	734	τwCH_2(C6),τwCH_2(C5)	739	τwCH_2(C6),τwCH_2(C5)
735 s		732	βR_2(A2), νC12-C14	729	βR_2(A2)	730	βR_2(A2)
	719 vw	712	τwCH_2(C10), τwCH_2(C9)	709	τR_1(A2)	712	τwCH_2(C9), τwCH_2(C10)
703 s		703	τR_1(A2)	699	τwCH_2(C10)	700	τR_1(A2)
	672 vw	695	τR_1(A3)	693	τR_1(A3)	695	τR_1(A3)
647 w		660	τR_1(A2)	660	ρC12=O1	660	τR_1(A2)
	639 s	636	βR_2(A2), νC12-C14	636	βR_2(A2)	641	βR_2(A2), ρC12=O1,νC12-C14
		632	βR_2(A3), βR_3(A3)	631	βR_2(A3), βR_3(A3)	631	βR_2(A3), βR_3(A3)
		630	βR_3(A2)	630	βR_3(A2)	628	βR_3(A2)
607 w	592 vw	605	βR_3(A3), τR_1(A3)	602	βR_3(A3), τR_1(A3)	602	βR_3(A3), τR_1(A3)
578 m		561	γC12=O1, τwCH_2(C14)	561	τwCH_2(C14)	562	τwCH_2(C14)
542 w		542	τR_3(A2), τR_1(A2)	534	τR_3(A2), τR_1(A2)	536	βR_1(A1)
511 m		512	τR_2(A3), γC10-C13	505	τR_2(A3), γC10-C13	510	τR_2(A3),γC10-C13
		496	βR_2(A1), τR_2(A3)	494	βN3-C11, βR_2(A1)	488	βR_2(A1)
475 w	483 m	480	τR_3(A2)	470	τR_3(A2), τR_2(A3)	474	βR_3(A1)
		463	βR_3(A1)	460	βR_3(A1)	455	βR_3(A1),βR_2(A1)
450 m	454 w	447	βN3-C11,βR_2(A1)	445	βR_2(A1), βN3-C11	432	βN3-C11
	426 m	410	τR_2(A2)	426	γC9-N2	426	γC9-N2
		404	τR_1(A1), δC14C12N3	412	τR_2(A2)	409	τR_2(A2)
		402	τR_3(A3)	402	τR_3(A3)	401	τR_3(A3)
398 m	393 w	389	γC9-N2	399	δC14C12N3	398	βR_2(A2), νN3-C11
		369	βC9-N2	361	βC9-N2	371	βC9-N2
	346 sh	332	βC10-C13	322	βC10-C13	337	βC10-C13
	294 s	298	δC12C14C17	300	τR_3(A2)	303	νN3-C12
		286	δC14C12N3,δC12C14C17	286	δC13C10C9	292	δC12C14C17,δC4N3C12
		285	τR_1(A1)	281	τR_1(A1)	276	τR_3(A2), τR_2(A3)
		264	δN3C4C5	264	δN3C4C5	268	τR_1(A1), δN3C4C5
		244	δN3C4C6	240	δN3C4C6	242	τR_3(A2),δC14C12N3,δN3C4C6
		230	τR_3(A1),τR_2(A1)	215	τR_3(A1)	226	τR_3(A1),τR_2(A1)
				209	τwCH_3	207	νH54-Cl55
		198	τwCH_3, τR_2(A3)	193	τR_3(A1), τR_2(A3)	196	τwCH_3
		189	τwCH_3			186	τwCH_3
		174	δC14C12N3, δC4N3C12	167	δC10C9N2	163	δC10C9N2
		115	γC4-N3, βR_3(A1)	115	δC4N3C12	119	βR_3(A1), δC4N3C12
		93	τ_wC9-N2	92	γC4-N3	101	τ_wC9-N2
		88	γC4-N3	86	γN3-C11,ρC4-N3	87	γC4-N3
				81	τ_wC12-N3	79	δN2-H54-Cl55
		73	τ_wC12-N3, τ_wC9-N2			75	τ_wC12-N3
		68	τ_wC12-N3	62	τ_wN3-C11	73	τ_wC12-N3,τ_wC9-N2
		58	δC13C10C9,ρC4-N3	60	τ_wC9-N2,τ_wC10-C13	62	γN3-C11,ρC4-N3, δC13C10C9
		51	τ_wN3-C11	50	τ_wC9-N2,τ_wC10-C13	47	τ_wN3-C11
		38	τ_wC14-C12	40	τ_wC14-C12	43	τ_wC14-C12
		32	τ_wC10-C13	32	τ_wC10-C13	33	τ_wC14-C12,τ_wN3-C11
		25	τC9-C10	27	τ_wC9-N2,τC9-C10	29	τC9-C10,τR_2(A1)
		19	τ_wN3-C4, τR_2(A1)	20	τR_2(A1)	26	τ_wC10-C13
						15	τC9-C10
		14	τ_wN3-C4	14	τ_wN3-C4[#]	13	τ_wN3-C4

Abbreviations: □, stretching; □□□ deformation in the plane; □□□ deformation out of plane; wag, wagging; □□□□torsion; β_R, deformation ring τ_R, torsion ring; ρ, rocking; τw, twisting; δ, deformation; a, antisymmetric; s, symmetric; (A_1), Ring 1; (A_2), Ring R2; A_3, Ring R3; [a]This work, [b]From scaled quantum mechanics force field, [c]From Ref [38] for hydrochloride fentanyl. [#]Assigned by GaussView.

3.7.1.2 2000-1000 cm^{-1} range. The νC12=O1 and νC=C modes with double bonds characters of fentanyl species are assigned among 1653 and 1537 cm^{-1}, as predict by SQM calculations while the νC-C and νN-C modes with partial double and simple bonds are assigned from 1384 to 1006 cm^{-1}. The in-plane deformation or rocking modes (βC-H) are assigned among 1480 and 1147 cm^{-1} [20, 37]. Here, it is very important to mention that the vibration modes of aliphatic C-H groups (ρC-H) are in hybridization sp^3 and they are differenced from the aromatic ones with hybridization sp^2 by using the Greek letter ρho. The CH_3 deformation, rocking and twisting modes are assigned according to SQM calculations and, in accordance to similar species [20, 37]. In the same way, the CH_2 deformation, wagging and twisting modes, as observed in Table 5. Some deformations and torsions modes of three rings (βR_1 and τR_1) are also assigned around 1088 and 1017 cm^{-1} region, as predicted by SQM calculations.

3.7.1.3. 1000-10 cm^{-1} range. The νC-C and νN-C stretching modes with simple bonds characters in the three species of fentanyl are also predicted and assigned among 998 and 303 cm^{-1}. Remaining deformations and torsions modes of three rings are predicted by SQM calculations in this region. Here, the νH54-Cl55 stretching mode of hydrochloride fentanyl is

predicted at 207 cm^{-1} but this mode was not assigned because the experimental Raman spectrum was recorded up to 290 cm^{-1}. For the same reason, the assignments of many skeletal modes predicted in the complete region only are assigned up to 294 cm^{-1}, as indicated in Table 5. In the cationic species, the τ_wN3-C4 mode, identified by the symbol # in Table 5, was not predicted by SQM calculations but assigned by the *GaussView* program at 14 cm^{-1}, as in the other species of fentanyl [26].

4. Force Fields

Forces of diverse bonds in the fentanyl species should be analysed because they have shown diverse characteristics, in particular, the N2-H54 bonds of cation and hydrochloride evidenced different assignments. The presence of Cl54 in the hydrochloride in the two media have clear influence on the H54-Cl55 bonds and its properties. Therefore, for the fentanyl species the scaled force constants were computed using the harmonic force fields [23-25]. The results in both media are given in Table 6. First, the comparisons of *f(νN-H)* force constants for the species, with exception of the free base, show that the hydrochloride show lower values in both media than the cationic ones. The different nature of N2-H54 bonds justify these results because in the hydrochloride this bond is connected to Cl55 while in the cation the N2 of this bond is protonated. In both species, positive MK charges on N2 were observed (see Tables S1-S3 and Figs. 4a and 4b). The Cl in hydrochloride makes important variations in the *f(νC-N2)* and *f(νC-N3)* force constants in both media, as detected from Table 6. In addition, the lower values of *f(νC-N2)* force constants in those two species of fentanyl are obviously related to the positive charges on N2 and to the N2-H54 bonds. The *f(νC=O)* force constants of three species diminish in solution because they as acceptors of H bonds are hydrated in this medium with water molecules. On the contrary, the stretching $f(\nu CH_2)$ and $f(\nu CH_3)$ force constants and the corresponding to deformations modes remain practically constants in the three species and in both environments, indicating the little influence of Cl and the medium on their values. In the same way, the $f(\nu C\text{-}H)_{R2,R3}$ and $f(\nu C\text{-}C)_{R2,R3}$ force constants of both R2 and R3 rings in the three species of fentanyl show few changes in the values. Here, it is very important to mention that the *f(νH-Cl)* force constant of hydrochloride change from 0.81 mdyn $Å^{-1}$ in GP to 0.26 mdyn $Å^{-1}$ due to that this region is also hydrated in solution, as revealed by the intense red colour on Cl from its mapped MEP surface.

Table 6: Scaled internal force constants for the base, cation and hydrochloride fentanyl species in GP and AS using the B3LYP/6-311++G** method

Force constants	Fentanyl[a]					
	Free base		Cationic		Hydrochloride	
	Gas	PCM	Gas	PCM	Gas	PCM
f(νN-H)			5.96	5.89	3.04	4.95
$f(\nu C\text{-}H)_{R2,R3}$	5.08	5.10	5.09	5.09	5.08	5.10
f(νC=O)	10.90	9.35	11.10	9.66	10.84	9.44
$f(\nu CH_2)$	4.64	4.67	4.79	4.82	4.78	4.83
$f(\nu CH_3)$	4.83	4.81	4.86	4.82	4.83	4.81
$f(\nu C\text{-}C)_{R2,R3}$	6.35	6.31	6.36	6.33	6.35	6.32
f(νC-N2)	4.47	4.34	3.54	3.72	3.97	3.82
f(νC-N3)	4.95	5.04	4.91	5.10	4.98	5.06
f(νH-Cl)					0.81	0.26
$f(\delta CH_2)$	0.73	0.72	0.73	0.73	0.73	0.71
$f(\delta CH_3)$	0.53	0.52	0.53	0.53	0.53	0.52

Units are mdyn $Å^{-1}$ for stretching and mdyn Å rad^{-2} for angle deformations. [a]This work

Thus, the notable changes observed in AS, in reference to the values in GP, evidence clearly the hydration of acceptor (O and N atoms) and donor groups (N-H bond) of H bonds with water molecules.

5. Electronic spectrum

The experimental UV-visible spectrum of fentanyl in an acidic mobile phase at pH = 3 taken from Ref. [39] is related with the obtained for the base, cation and hydrochloride in AS by using the B3LYP/6-311++G** method and the Gaussian16 program [27]. These spectra are shown in Figure 11. Here, it is very important to know that fentanyl has no absorption in the visible region of 400−700 nm, as reported by Lin *et al*. [42]. The experimental spectrum shows a maximum at 205 nm with other weak band at 258 nm while in the predicted spectra of free base, cationic and hydrochloride species in AS are observed maxima respectively at 242, 256 and 291 nm. Here, the cation is clearly observed in AS because in this medium the base is protonated while the hydrochloride is present as cation. Here, these bands are connected to π→π* transitions due to C=C double bonds of phenyl rings, as suggested by NBO calculations and with comparable compounds [39-42].

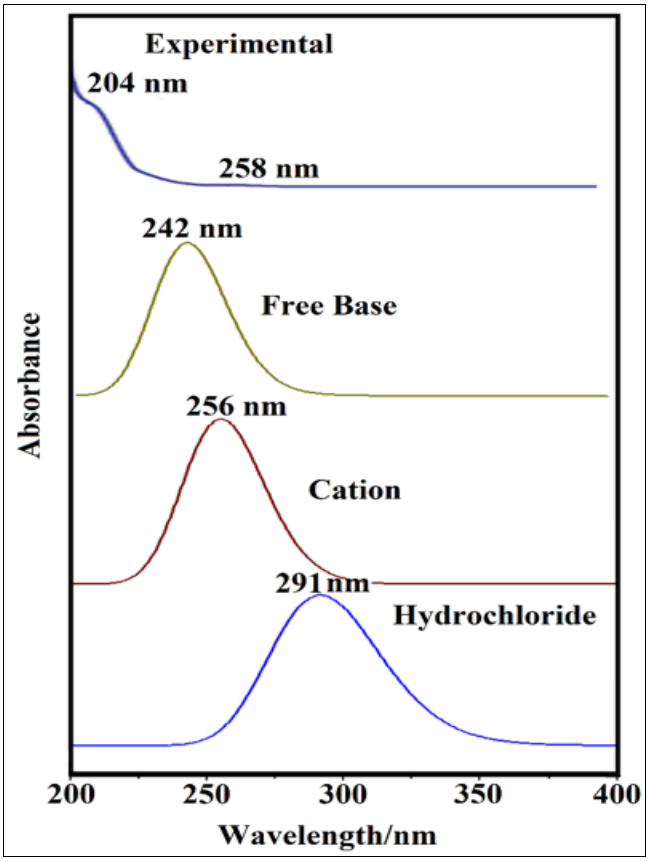

Fig 11: Experimental electronic spectrum of fentanyl in an acidic mobile phase at pH = 3 taken from Ref. [39] related to the predicted for the base, cation and hydrochloride in AS using B3LYP/6-311++G** level of theory

6. NMR study

In Tables 7 and 8 are shown the experimental ^{1}H and ^{13}C NMR chemical shifts of free base of fentanyl in $CDCl_3$ taken from Ref [40] compared with the predicted for the base, cation and hydrochloride fentanyl in AS using the GIAO method [36] and RMSD values. For some H and C nucleus the δ values are overvalued in reference to the experimental ones, hence, for the ^{1}H nucleus it is observed a better concordance with δ values between 0.49 and 0.26 ppm where the best correlation is observed for the free base, as expected because the experimental value is considered for this species. However, for the ^{13}C nucleus the RMSD values slightly increase.

Table 7: Observed and calculated ^{1}H chemical shifts (δ in ppm) for the three fentanyl forms in AS using the B3LYP/6-311++G** method compared with the experimental of base

B3LYP/6-311++G** method				Exp[b].
Atoms	Free base	Cation	Hydrochloride	
H26	5.20	5.58	4.75	4.62
H27	1.45	1.55	2.59	1.37
H28	1.46	2.11	1.89	1.74
H29	1.51	2.14	1.40	1.74
H30	1.42	1.52	1.77	1.37
H31	2.05	3.14	2.38	2.10
H32	2.61	3.28	3.23	2.94
H33	3.11	3.87	3.56	2.94
H34	1.73	2.90	2.22	2.10
H35	1.88	2.92	2.12	2.47
H36	2.33	2.96	2.89	2.47
H37	2.62	3.00	2.34	2.66
H38	2.55	2.47	4.03	2.66
H39	1.65	1.75	1.66	1.86
H40	1.63	1.72	1.77	1.86
H41	7.22	7.15	7.08	7.01
H42	7.22	7.16	7.30	7.01
H43	0.47	0.76	0.52	0.94
H44	1.03	1.15	1.04	0.94
H45	1.10	1.21	1.13	0.94
H46	7.31	7.31	7.18	7.08
H47	7.31	7.24	7.67	7.08
H48	7.54	7.78	7.55	7.32
H49	7.54	7.79	7.71	7.32
H50	7.56	7.89	7.68	7.30
H51	7.40	7.78	7.41	7.19
H52	7.41	7.76	7.57	7.19
H53	7.26	7.76	7.37	7.11
H54		2.80	11.36	
RMSD[b]	**0.26**	**0.49**	**0.46**	

[a]This work, [b]From Ref [40] in $CDCl_3$

Thus, when the ^{13}C NMR chemical shifts are compared for the three species, the RMSD values increase to values among 5.74 and 4.78 ppm. These modifications are rapidly justified by the calculations because the 6-311++G** basis set produce improved relationships for the H nuclei instead C atoms. Besides, the solvent used in the calculations to predict the ^{1}H and ^{13}C NMR chemical shifts of three species are different from that experimental.

Table 8: Observed and calculated ^{13}C chemical shifts (δ in ppm) for the three fentanyl forms in AS using the B3LYP/6-311++G** method compared with the experimental of base

B3LYP/6-311++G** method				Exp[b].
Atoms	Free base	Cation	Hydrochloride	
C4	54.68	49.76	54.80	52.29
C5	33.21	32.33	28.57	30.73
C6	32.60	31.82	29.78	30.73
C7	59.52	61.15	58.39	53.32
C8	55.30	57.68	53.41	53.32
C9	67.68	65.73	64.63	60.72
C10	38.77	36.89	33.12	34.03
C11	147.38	143.16	145.68	139.02
C12	178.84	181.51	180.61	173.80
C13	148.35	135.15	143.53	140.40
C14	32.39	33.42	32.55	28.76
C15	137.49	135.92	135.35	130.67
C16	137.60	136.04	136.72	130.67
C17	9.31	9.10	9.07	9.86
C18	134.19	133.14	133.46	128.87
C19	133.86	132.69	135.45	128.87
C20	134.02	136.21	134.36	129.54
C21	134.05	136.27	136.56	129.54
C22	132.85	136.31	134.69	128.52
C23	133.74	136.81	133.62	128.63
C24	133.53	136.67	135.05	128.63
C25	130.46	136.43	132.16	126.29
RMSD[b]	**5.11**	**5.74**	**4.78**	

[a]This work, [b]From Ref [40] in $CDCl_3$

7. Conclusions

Here, the theoretical molecular structures of base, cation and hydrochloride forms of potent opioid analgesic fentanyl drug were determined in GP and in AS using hybrid B3LYP/6-311++G** calculations. Structural, electronic, topological and vibrational properties were predicted for the species in different media. The cation shows higher solvation energy (-294.42 kJ/mol) than the other ones. However, the three fentanyl species show values comparable to morphine, cocaine, scopolamine and heroin alkaloids by using the B3LYP/6-31G* level of theory. Positive atomic MK charges on N2 confirm that the protonation of cationic and hydrochloride species takes place on N2 of piperazine ring. The most reactive species with low kinetic stability and lower gap value (4.4545 eV) is observed clearly for the hydrochloride species in solution while the cation in the gas phase is the less reactive (5.4940 eV). Probably, the higher stabilization energy of hydrochloride form in solution justify its low kinetic stability, as supported by NBO calculations.

Complete assignments of the expected 153, 156 and 159 normal vibration modes for the base, cation and hydrochloride fentanyl and its scaled force constants are reported by using the harmonic force fields and the SQMFF methodology. Very good correlations evidence the predicted spectra when are related to the experimental ones. However, the absence of very intense IR band in the experimental spectrum predicted for the hydrochloride form at 1913 cm^{-1} by using SQM calculations and, that in the Raman spectrum is observed with lower intensity, evidence the presence of cation in the solid phase and in As. In the same way, the electronic spectra for the base and hydrochloride forms reveal that the cation is present in AS, as suggested by the corresponding experimental.

8. Availability of data

All data generated or analysed during this study are included in this published article.

9. Code availability

Not applicable.

10. Consent to participate
Not applicable.

11. Consent for publication
Not applicable.

12. CRediT authorship contribution statement
Elida Romano: Data curation, formal analysis and methodology, Maximiliano A. Iramain: Data curation, María E. Manzur: Data curation, María V. Castillo: Conceptualization, formal analysis and methodology, Silvia Antonia Brandán: Methodology, supervision and Writing, review and editing.

13. Declaration of competing interest
The authors declare that they have no known competing financial interests or personal relationships that could have appeared to influence the work reported in this paper.

14. Data availability
Data will be made available on request.

15. Acknowledgements
This work was subsidized with grants from Project N° D714 (Consejo de Investigaciones, Universidad Nacional de Tucumán). The authors thank Prof. Sundius for his permission to use MOLVIB.
Supporting Information available: Tables S1-S7 and Figures S1-S2.

16. References
1. Scholz J, Steinfath M, Schulz M. Clinical pharmacokinetics of alfentanil, fentanyl and sufentanil. An update, Clin Pharmacokinet. 1996; 31(4):275-292. Doi: https://doi.org/10.2165/00003088-199631040-00004.
2. Ogawa N, Nagase H, Endo T, Loftsson T, Ueda H. Crystal Structure of Fentanyl Base, X-ray Structure Analysis Online. 2009; 25.
3. Asadi Z, Esrafili MD, Vessally E, Asnaashariisfahani M, Yahyaei S, Khani A. A structural study of fentanyl by DFT calculations, NMR and IR spectroscopy, J. Mol. Struct. 2017; 1128:552-562. Doi: https://doi.org/10.1016/j.molstruc.2016.09.027.
4. Ramsay M. Fentanyl Detection and Quantification Using Portable Infrared Absorption Spectroscopy, Thesis, B.Sc., University of Victoria, 2018.
5. Sridharan K, Sivaramakrishnan G. Comparison of Fentanyl, Remifentanil, Sufentanil and Alfentanil in Combination with Propofol for General Anesthesia: A Systematic Review and Meta-analysis of Randomized Controlled Trials. Curr Clin Pharmacol. 2019; 14(2):116-124. Doi: https://doi.org/10.2174/1567201816666190313160438.
6. Xu M, Wang C-H, Terracciano AC, Masunov AE, Vasu SS. High accuracy machine learning identification of fentanyl-relevant molecular compound classification via constituent functional group analysis, Sci Rep. 2020; 10:13569. Doi: https://doi.org 10.1038/s41598-020-70471-7.
7. Winokur AD, Kaufman LM, Almirall JR. Differentiation and identification of fentanyl analogues using GC-IRD. Forensic Chemistry. 2020; 20:100255. Doi: https://doi.org/10.1016/j.forc.2020.100255.
8. Sinhorini LFC, Rodrigues CHP, Leite VBP, Bruni AT. Synthetic fentanyls evaluation and characterization by infrared spectroscopy employing in silico methods. Computational and Theoretical Chemistry. 2021; 1204:113378. Doi: https://doi.org/10.1016/j.comptc.2021.113378.
9. Ramsay M, Gozdzialski L, Larnder A, Wallace B, Hore D. Fentanyl quantification using portable infrared absorption spectroscopy. A framework for community drug checking. Vibrational Spectroscopy. 2021; 114:103243. Doi: https://doi.org/10.1016/j.vibspec.2021.103243.
10. Swanson KD, Shaner RL, Krajewski LC, Bragg WA, Johnson RC, Hamelin EI. Use of Diagnostic Ions for the Detection of Fentanyl Analogs in Human Matrices by LC-QTOF, J Am Soc Mass Spectrom. 2021; 32(12):2852-2859. Doi: https://doi.org/10.1021/jasms.1c00267.
11. Lin X, Hong-yuan H, Cui-mei L, Zhen-dong H. Study on Vibrational Spectral Characteristics of Fentanyl-Class Substances, Spectroscopy and Spectral Analysis. 2021; 41(9):2829-2834. Doi: https://doi.org/10.3964/j.issn.1000-0593(2021)09-2829-06.
12. Shan X, Lee L, Clewes RJ, Howle CR, Sambrook MR, Clary DC. Computational analyses of the vibrational spectra of fentanyl, carfentanil and remifentanil, Spectrochimica Acta Part A: Molecular and Biomolecular Spectroscopy. 2022; 270:120763. Doi: https://doi.org/10.1016/j.saa.2021.120763.
13. Ferguson K, Perr J, Tupik S, *et al*. An Interlaboratory Study to Evaluate the Utility of Gas Chromatography–Mass Spectrometry and Gas Chromatography–Infrared Spectroscopy Spectral Libraries in the Forensic Analysis of Fentanyl-related Substances, J. For. Sci. 2023; 68(5):1504-1519. Doi: https://doi.org/10.1111/1556-4029.15306.
14. Crepeault H, Socias ME, Tobias S, Lysyshyn M, Custance A, Shapiro A, Ti L. Examining fentanyl and its analogues in the unregulated drug supply of British Columbia, Canada using drug checking technologies, Drug Alcohol Rev. 2023; 42(3):538-543. Doi: https://doi.org/10.1111/dar.13580.
15. Wilcox PG, Emmons ED, Pardoe IJ, Kline ND, Guicheteau JA. Quantitative Raman Cross-Sections and Band Assignments for Fentanyl and Fentanyl Analogs. 2023; 77(5):439-448. Doi: https://doi.org/10.1177/00037028231160565.
16. Dogruer ES, Hernandez E, Cruz J, Mebel AM, McCord B. Differentiating Structurally Similar Fentanyl Analogs by Comparing Density Functional Theory (DFT) Calculations and Surface-Enhanced Raman Spectroscopy (SERS) Results. Appl Spectrosc. 2024; 78(7):667-679. Doi: https://doi.org/10.1177/00037028241246010.
17. Barney A, Trojan V, Hrib R, Newland A, Halámek J, Halámková L. From Spectra to Signatures: Detecting Fentanyl in Human Nails with ATR–FTIR and Machine Learning, Sensors. 2025; 25(1):227. Doi: https://doi.org/10.3390/s25010227.
18. Muñoz Reyes DM, Restrepo Zapata JH. Detection of Fentanyl and its Analogues Using Portable Raman Spectroscopy in the Monitoring of Fraudulent Activities Systematic Review, Pharmacy and Drug Development.

2025; 4(1). Doi: https://doi.org/10.58489/2836-2322/PDD.
19. Malone MW, Mason HE, Altenhof AR, Espy MA, Alvarez MA, Batrice RJ, *et al*. Detection of fentanyl hydrochloride via nuclear quadrupole resonance: A multimodality pursuit, PNAS Nexus. 2025; 4(7):190. Doi: https://doi.org/10.1093/pnasnexus/pgaf190
20. Rudyk RA, Checa MA, Catalán CAN, Brandán SA. Structural, FT-IR, FT-Raman and ECD spectroscopic studies of free base, cationic and hydrobromide species of scopolamine alkaloid, J. Mol. Struct. 2019; 1180:603-617. Doi: https://doi.org/10.1016/j.molstruc.2018.12.040.
21. Becke AD. Density-functional exchange-energy approximation with correct asymptotic behavior, Phys. Rev. 1988; A38(6):3098-3100. Doi: https://doi.org/10.1103/physreva.38.3098.
22. Lee C, Yang W, Parr RG. Development of the Colle-Salvetti correlation-energy formula into a functional of the electron density, Phys. Rev. 1988; B37:785-789. Doi: https://doi.org/10.1103/physrevb.37.785.
23. Pulay P, Fogarasi G, Pongor G, Boggs JE, Vargha A. Combination of theoretical ab initio and experimental information to obtain reliable harmonic force constants. Scaled quantum mechanical (QM) force fields for glyoxal, acrolein, butadiene, formaldehyde, and ethylene. J. Am. Chem. Soc. 1983; 105:7073. Doi: https://doi.org/10.1021/ja00362a005.
24. Rauhut G, Pulay P. Transferable Scaling Factors for Density Functional Derived Vibrational Force Fields, J. Phys. Chem. 1995; 99:3093-3100. Doi: https://doi.org/10.1021/j100010a019
25. Sundius T. Scaling of ab-initio force fields by MOLVIB. Vib. Spectrosc. 2002; 29(9):89-95. Doi: https://doi.org/10.1016/S0924-2031(01)00189-8.
26. GaussView, version 6.1.1, R.D. Dennington, T.A. Keith, J.M. Millam, Semichem Inc., Shawnee Mission, KS, 2019.
27. Frisch MJ, Trucks GW, Schlegel HB, Scuseria GE, *et al*. Gaussian 16. Revision C.01. Inc., Wallingford CT, 2019.
28. Marenich AV, Cramer CJ, Truhlar DG. Universal solvation model based on solute electron density and a continuum model of the solvent defined by the bulk dielectric constant and atomic surface tensions, J. Phys. Chem. 2009; B113(18):6378-6396. Doi: https://doi.org/10.1021/jp810292n.
29. Ugliengo P. MOLDRAW Program, University of Torino, Dipartimento Chimica IFM, Torino, Italy, 1998.
30. Glendening E, Badenhoop JK, Reed AD, Carpenter JE, Weinhold F. NBO 3.1; Theoretical Chemistry Institute, University of Wisconsin; Madison, WI, 1996.
31. Bader RFW. Atoms in Molecules, A Quantum Theory, Oxford University Press, Oxford, 1990. ISBN 0198558651.
32. Biegler-Köning F, Schönbohm J, Bayles D. AIM 2000; A program to Analyze and Visualize atoms in molecules, J. Comput. Chem. 2001; 22:545. Doi: https://doi.org/10.1002/1096-987X(20010415)22:5<545::AID-JCC1027>3.0.CO;2-Y.
33. Pearson RG. Absolute electronegativity and hardness correlated with molecular orbital theory, Proc. Natl. Acad. Sci. U.S.A. 1986; 83:8440-8441. Doi: https://doi.org/10.1073/pnas.83.22.8440.
34. Parr RG, Szentpaly LV, Liu S. Electrophilicity index, J. Am. Chem. Soc. 1999; 121:1922-1924. Doi: https://doi.org/10.1021/ja983494x.
35. Keresztury G, Holly S, Besenyei G, Varga J, Wang AY, Durig JR. Vibrational spectra of monothiocarbamates-II. IR and Raman spectra, vibrational assignment, conformational analysis and ab initio calculations of S-methyl-N,N-dimethylthiocarbamate. Spectrochim. Acta. 1993; 49A:2007-2026.
36. Ditchfield R. Self-consistent perturbation theory of diamagnetism. I. A gauge-invariant LCAO (linear combination of atomic orbitals) method for NMR chemical shifts, Mol Phys. 1974; 27:714-722.
37. Manzur ME, Brandán SA. S(-) and R(+) Species Derived from Antihistaminic Promethazine Agent: Structural and Vibrational Studies, Submitted to Heliyon. 2019; 5:e02322. Doi: https://doi.org/10.1016/j.heliyon.2019.e02322
38. Available from: Web page: https://webbook.nist.gov/cgi/cbook.cgi
39. Lin Y, Sun J, Tang M, Zhang G, Yu L, Zhao X, *et al*. Synergistic Recognition-Triggered Charge Transfer Enables Rapid Visual Colorimetric Detection of Fentanyl, Anal. Chem. 2021; 93:6544-6550. Doi: https://doi.org/10.1021/acs.analchem.1c00723.
40. Available from: Web page: https://SIELC.com/fentanyl
41. Mitchell CK, Dumke JC, Corbett CA, Jones LM, Ceniccola-Campos KE. The quantitative and qualitative analysis of dye in fentanyl tablets via ultraviolet-visible spectroscopy-A forensic approach. J Forensic Sci. 69(6):2222-2229. Doi: https://doi.org/10.1111/1556-4029.15598
42. Jimeno ML, Alkorta I, Cano C, Jagerovic N, Goya P, Elguero J, *et al*. Fentanyl and Its Analogue N-(1-Phenylpyrazol-3-yl)-N-[1-(2-phenylethyl) 4-piperidyl]propanamide: 1H- and 13C-NMR Spectroscopy, X-Ray Crystallography, and Theoretical Calculations, Chem. Pharm. Bull. 2003; 51(8):929-934.